PAPER

Check for updates

Pyrene-based covalent organic polymers with nano carbonaceous composites for efficient supercapacitive energy storage†

Mohsin Ejaz, [ID] ‡[a] Mohamed Gamal Mohamed, [ID] ‡*[ab] Wei-Chun Huang[a] and Shiao-Wei Kuo [ID] *[ac]

Covalent organic polymers (COPs) show great potential as supercapacitor electrodes due to their tunable properties, stability, and high capacitance. In this work, we prepared a covalent organic polymer (Py-DSDA-COP) through a Schiff base reaction of the 1,3,6,8-tetrakis(4-formylphenyl)pyrene monomer (Py-Ph-CHO) and 4,4′-disulfanediyldianiline (DSDA), validated its chemical structure, and investigated its thermal stability, porosity, morphology, and electrochemical properties. The Py-DSDA-COP displayed high semi-crystallinity, good porosity, and a specific capacitance of 56.18 F g^{-1}. To improve its electrochemical performance, we incorporated different nano-carbonaceous materials [fullerene (C60), MWCNTs, and SWCNTs] into Py-DSDA-COP and compared their characteristics. The Py-DSDA-COP/SWCNTs showed the highest specific capacitance (171 F g^{-1}) at 1 A g^{-1} and highest energy density (23.7 W h kg^{-1}) with a capacity retention of 93% after 2000 cycles, which is superior to those of Py-DSDA-COP/MWCNTs and Py-DSDA-COP/C60 nanocomposites. These superior electrochemical characteristics of Py-DSDA-COP/SWCNTs are attributed to the excellent $\pi-\pi$ stacking interactions, higher EDLC behavior, higher conductivity, lower diameter, and higher surface area of SWCNTs than those of MWCNTs.

Introduction

Covalent organic polymers (COPs) are a class of organic materials composed of repeating units linked by covalent bonds, resulting in a three-dimensional network structure.[1–6] They are typically made up of light elements such as carbon, nitrogen, and oxygen, and can have diverse chemical structures, allowing for a wide range of properties and potential applications.[7–12] In recent years, there has been a growing amount of attention towards COPs because of their unique properties, including high surface area, tunable porosity, and chemical stability.[13–20] COPs can also be synthesized in a variety of ways, including through the polymerization of small molecules or through self-assembly of pre-formed building blocks.[21–25] Some potential applications of COPs include gas storage materials for hydrogen and carbon dioxide,[26–28] heterogeneous catalysts for organic

reactions,[29–31] and electrode materials for supercapacitors and battery devices.[32–35] Supercapacitors (SCs), in particular, have emerged as potential electrochemical energy storage systems and have gained popularity due to their outstanding high-power density, quick charge/discharge processes, exceptional stability, and environmental friendliness.[36–45] They have the capability to perform like batteries and traditional capacitors. Electrostatic interactions between the electrolyte ions and the carbon electrodes lead to storing energy in them. One of the key advantages of COPs for supercapacitor applications is their high surface area, which can be tuned by adjusting the size and shape of the monomers used to synthesize the polymer.[46–48] The significant surface area offered by these materials provides numerous active sites for electrochemical reactions to occur which can enhance the energy storage capacity of the supercapacitor.[49,50] Additionally, COPs can be easily synthesized using simple and cost-effective methods, which makes them attractive for large-scale production. However, one of the current limitations of COPs for supercapacitor applications is their relatively low electrical conductivity, which can limit their charge/discharge rate.[51–54] Incorporating conducting carbon materials (such as CNTs and graphene) into COFs, CMPs, and MOFs is an effective way to boost their conductivity, improving their electrochemical performance.[55–58] The Py-OXD-CMP/CNT nanocomposites prepared by our group have exhibited a capacitance of 504 F g^{-1}.[55] In addition, our group has developed the TBN-Py-CMP/

[a]Department of Materials and Optoelectronic Science, Center for Functional Polymers and Supramolecular Materials, National Sun Yat-Sen University, Kaohsiung 804, Taiwan. E-mail: mgamal.eldin12@yahoo.com; kuosw@faculty.nsysu.edu.tw

[b]Chemistry Department, Faculty of Science, Assiut University, Assiut 71515, Egypt

[c]Department of Medicinal and Applied Chemistry, Kaohsiung Medical University, Kaohsiung 807, Taiwan

† Electronic supplementary information (ESI) available. See DOI: https://doi.org/10.1039/d3ta02741d

‡ These authors equally contributed.

(a)

Py-Ph-CHO

(b)
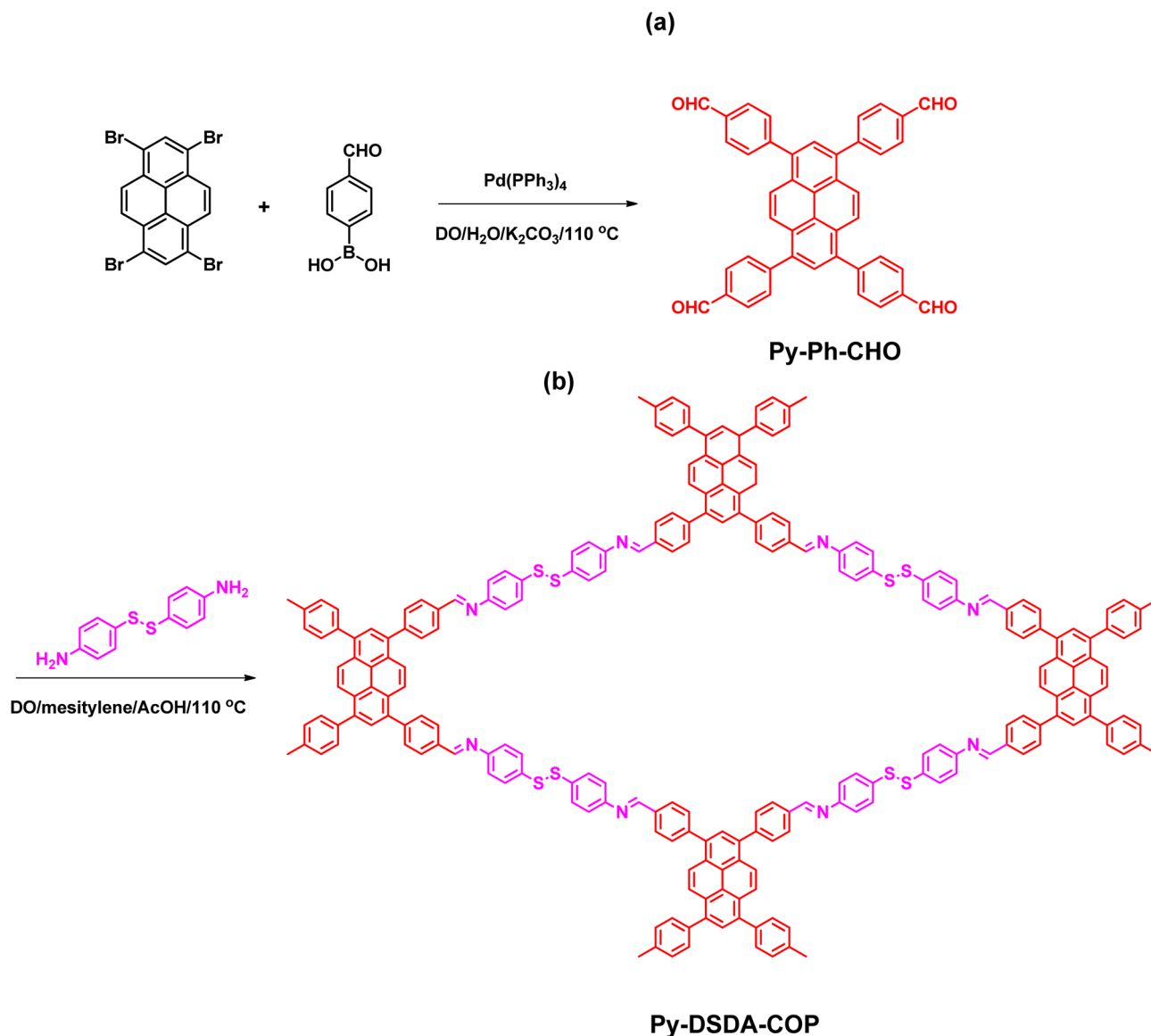
Py-DSDA-COP

Scheme 1 Synthesis of (a) Py-Ph-CHO and (b) Py-DSDA-COP.

CNT nanocomposite, which has exhibited a specific capacitance of 430 F g^{-1}.[56]

The Duan group found a capacitance of 365 F g^{-1} for a CoPc-CMP/CNT material.[57] Lin *et al.* synthesized a CNT@Mn-MOF composite for supercapacitor application.[58] We hypothesized that combining nano carbonaceous materials with COPs would be a suitable way to develop active electrode materials for supercapacitor application. Therefore, in this study, we blended three different carbon materials (fullerene (C60), MWCNTs, and SWCNTs) into Py-DSDA-COP to improve and compare the electrochemical performance of COP-based supercapacitors. The preparation of Py-DSDA-COP through Schiff base coupling of Py-Ph-CHO and 4,4'-disulfanediyldianiline (DSDA) is shown in Scheme 1. The chemical structure, thermal stability, nature, porosity, and electrochemical performance of three electrode systems and symmetric coin cells are discussed below in detail.

Experimental section

Materials

Potassium carbonate (K_2CO_3), sodium hydroxide (NaOH), pyrene (Py), 4-formylphenylboronic acid (4-FP-BO), and nitrobenzene ($C_6H_5NO_2$) were purchased from Sigma-Aldrich. Mesitylene, acetic acid (AcOH), 1,4-dioxane (DO), 4,4'-disulfanediyldianiline (DSDA), acetone, and tetrahydrofuran (THF) were obtained from Alfa Aesar.

Preparation of 1,3,6,8-tetrabromopyrene (Py-Br$_4$)

Py-Br$_4$ was obtained as a green solid (17 g) by refluxing 80 mL of $C_6H_5NO_2$, 8 g of Py (40 mmol), and Br$_2$ (9.2 mL, 176 mmol) at 120 °C for 24 hours, according to Scheme S1.† The FTIR spectrum (Fig. S1†): 3054 cm^{-1} (aromatic CH) and 681 cm^{-1} (C–Br).

This journal is © The Royal Society of Chemistry 2023

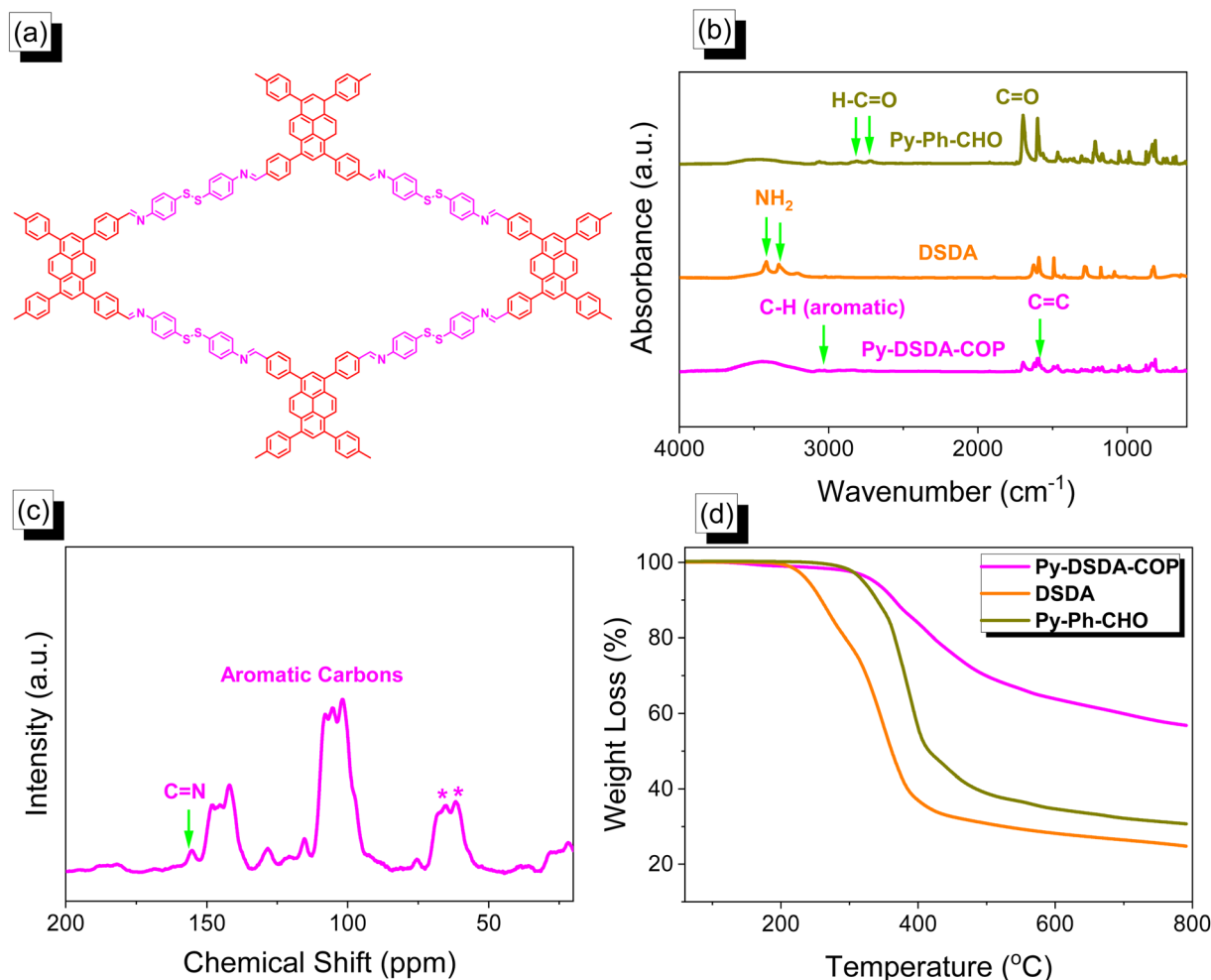*J. Mater. Chem. A*, 2023, **11**, 22868–22883 | **22869**

Fig. 1 (a) Chemical structure of Py-DSDA-COP. (b) FTIR spectra of Py-Ph-CHO, DSDA and Py-DSDA-COP. (c) Solid state ^{13}C NMR of Py-DSDA-COP. (d) TGA of Py-Ph-CHO, DSDA and Py-DSDA-COP.

Preparation of 1,3,6,8-tetrakis(4-formylphenyl)pyrene (Py-Ph-CHO)

4-FP-BO (4.40 g, 29.00 mmol), K_2CO_3 (5.30 g, 37.86 mmol), Py-Br$_4$ (2.50 g, 4.83 mmol), and Pd(PPh$_3$)$_4$ (0.23 g, 0.25 mmol) were refluxed in 80 mL of DO and 40 mL of H_2O at 110 °C under N_2 for 72 h. After working up the reaction mixture with 100 mL of HCl (2 N), a yellow solid was obtained which was washed with water and MeOH to yield pure Py-Ph-CHO [Scheme 1(a), 2.13 g]. FTIR (cm^{-1}, Fig. 1(a)): 3061, 2813–2732 (aldehydic CH), 1706 (C=O), and 1598 (C=C). ssNMR (Fig. S2†): 182.38 (CHO), 143.85–121.36 (aromatic carbons).
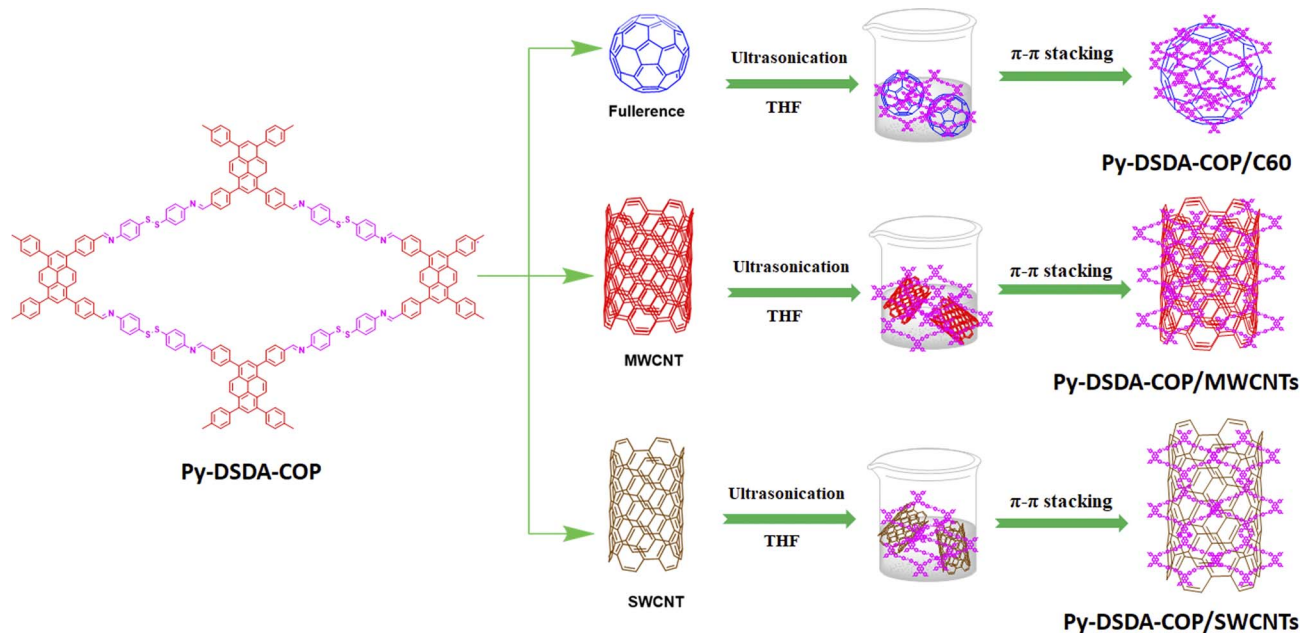
Preparation of Py-DSDA-COP

The solution of Py-Ph-CHO (0.15 g, 0.24 mmol), DSDA (0.12 g, 0.48 mmol), mesitylene (5 mL), acetic acid (0.65 mL), H_2O (0.35 mL), and DO (5 mL) was degassed two times under vacuum and then stirred at 75 °C for 72 h, filtered and washed with THF, H_2O, MeOH, and acetone to get a yellow solid, which was dried in a vacuum oven overnight.

Preparation of Py-DSDA-COP/nanocomposites

Py-DSDA-COP (2 wt%), and C60, MWCNTs, and SWCNTs (2 wt%) were individually dissolved in THF and sonicated overnight, and then the solvent was removed by rotary evaporation to afford Py-DSDA-COP/C60, Py-DSDA-COP/MWCNTs, and Py-DSDA-COP/SWCNTs nanocomposites, respectively as shown in Scheme 2.

Results and discussion

Pyrene is a polycyclic aromatic hydrocarbon that has been explored for various applications, including its potential use in energy storage due to its high electrical conductivity, surface area, porous structure, and redox activity. These characteristics make pyrene a good candidate to be used as an active electrode material for supercapacitors. The synthesis of a porous COP material based on Py-Ph-CHO and DSDA to afford Py-DSDA-COP is shown in Scheme 1. The Py-Ph-4CHO monomer was synthesized *via* the Suzuki coupling reaction of Py-Br$_4$ with 4-FP-BO in the presence of DO/K_2CO_3/H_2O at 110 °C for 72 h [Scheme 1(a)].

22870 | J. Mater. Chem. A, 2023, 11, 22868–22883

This journal is © The Royal Society of Chemistry 2023

Scheme 2 Preparation of Py-DSDA-COP/C60, Py-DSDA-COP/MWCNTs and Py-DSDA-COP/SWCNTs nanocomposites.

Finally, Py-DSDA-COP was obtained by a Schiff base reaction of Py-Ph-CHO and DSDA in the presence of dioxane/mesitylene at 110 °C [Scheme 1(b)]. The resultant porous Py-DSDA-COP material is insoluble in acetone, methanol, and THF. The chemical structure of Py-DSDA-COP [Fig. 1(a)] was validated through FTIR and ^{13}C solid-state NMR as shown in Fig. 1(b) and
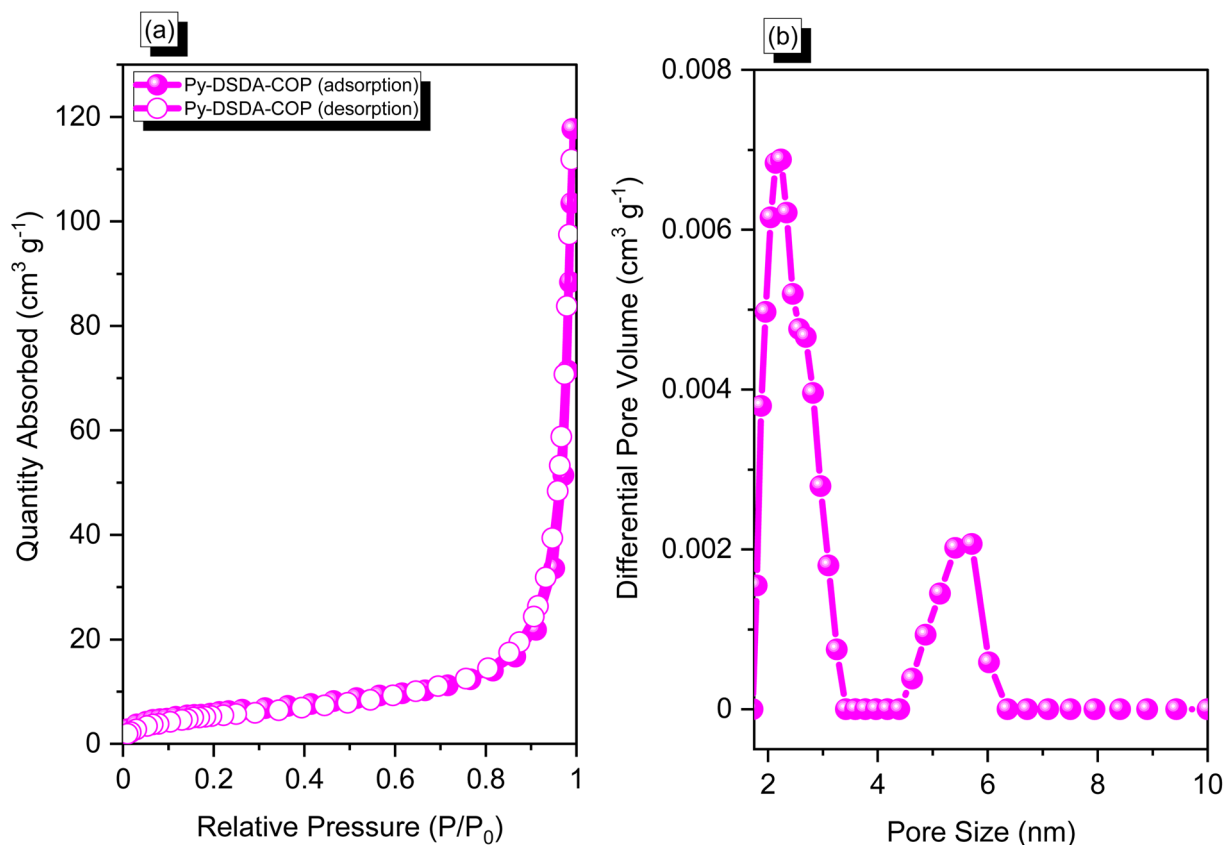
Fig. 2 (a) N_2 adsorption/desorption curve and (b) pore size of Py-DSDA-COP.

This journal is © The Royal Society of Chemistry 2023

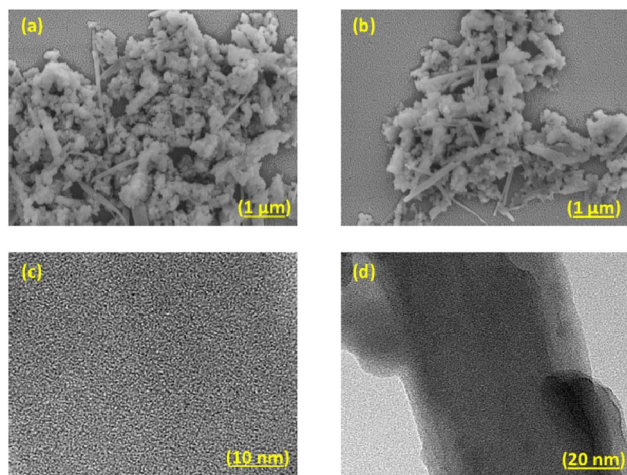J. Mater. Chem. A, 2023, 11, 22868–22883 | 22871

Fig. 3 SEM (a and b) and TEM images (c and d) of Py-DSDA-COP.

(c). The FTIR spectrum of Py-Ph-CHO showed peaks at 2813–2732 and 1706 cm^{-1}, representing the aldehydic C–H and C=O groups, respectively (Fig. 1(b)). The absorption bands of the NH$_2$ group in the DSDA monomer appeared at 3411 and 3328 cm^{-1}. The FTIR spectrum of Py-DSDA-COP showed a peak at 1605 cm^{-1} corresponding to C=N, with the complete absence of N–H and C=O peaks from the starting monomers Py-Ph-CHO and DSDA, respectively. Furthermore, Py-DSDA-COP exhibited a peak at 1592.11 cm^{-1} representing an aromatic C=C unit. The solid-state NMR of Py-DSDA-COP showed signals at 156.5 ppm for C=N and 148.5–128.0 ppm for aromatic carbons (Fig. 1(c)). The FTIR and NMR analyses confirmed the successful synthesis of Py-DSDA-COP. The thermal stabilities of Py-DSDA-COP and its ingredients (Py-Ph-CHO and DSDA) were measured through thermogravimetric analysis, as shown in (Fig. 1(d)).

The thermal decomposition temperature (T_{d5}, T_{d10}) and char yield were observed as 240 °C, 258 °C, and 25 wt% for DSDA, while 320 °C, 340 °C, and 31 wt% for Py-Ph-CHO, respectively. We observed that after the Schiff base reaction of Py-Ph-CHO and DSDA, the thermal stability of the resultant porous material (Py-DSDA-COP) improved. The values of T_{d5}, T_{d10}, and char yield were 335 °C, 360 °C, and 57 wt%, respectively. Moreover, FTIR analysis [Fig. S3†] of Py-DSDA-COP shows distinct peaks at 3058 and 1592.11 cm^{-1}, corresponding to the aromatic CH and C=C groups. These peaks serve as evidence of the robustness and integrity of the chemical structure of the Py-DSDA-COP framework, even after exposure to various temperatures ranging from 25 to 180 °C. Notably, the absence of an absorption peak at 2515 cm^{-1} in the Py-DSDA-COP FTIR spectrum, typically associated with –SH groups, further supports the stability of the S–S bond within the material.

The nature of the Py-DSDA-COP material was validated by the powder X-ray diffraction (XRD) pattern, as shown in Fig. S4.† The result revealed the semi-crystallinity behavior of Py-DSDA-COP from the existence of some sharp peaks in its XRD profile. The porosity of Py-DSDA-COP was examined by N$_2$ absorption at 77 K, as shown in Fig. 2. The Py-DSDA-COP showed a type II isotherm curve according to IUPAC. The Py-DSDA-COP exhibited rapid intake at high pressure demonstrating a mesoporous structure as shown in Fig. 2(a). Furthermore, we observe a S_{BET}, pore size, and pore volume of
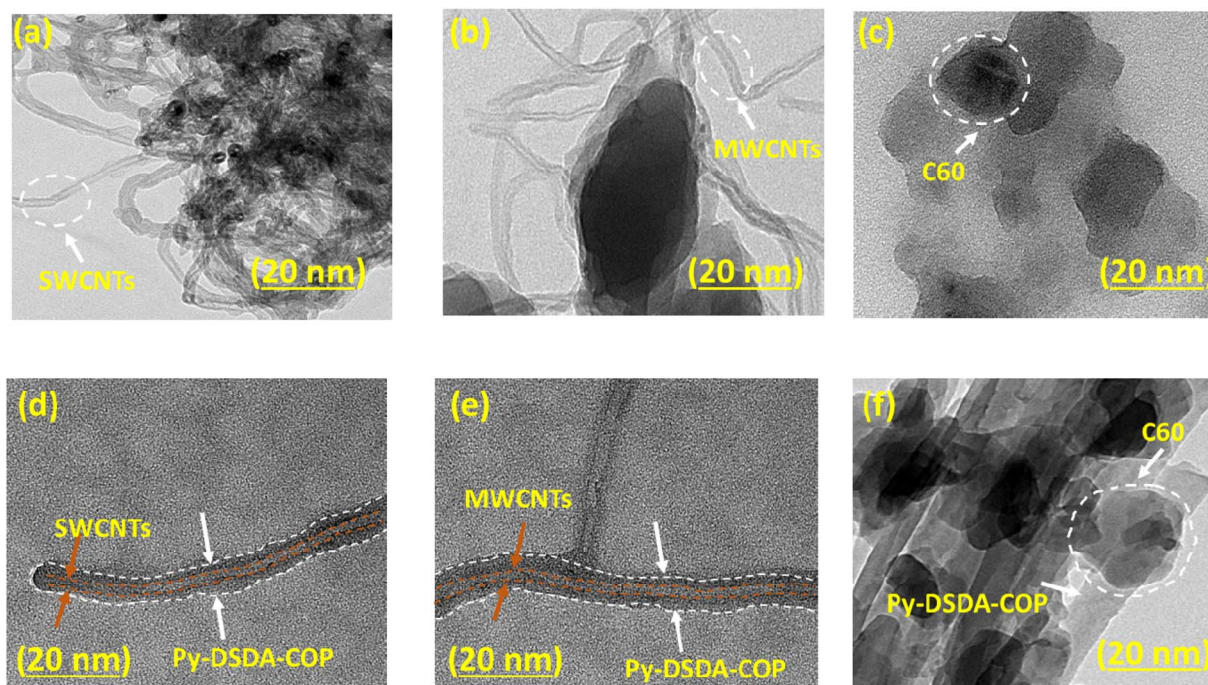

Fig. 4 TEM images of (a) SWCNTs, (b) MWCNTs, (c) C60, (d) Py-DSDA-COP/SWCNTs, (e) Py-DSDA-COP/MWCNTs and (f) Py-DSDA-COP/C60.

22872 | J. Mater. Chem. A, 2023, 11, 22868–22883

This journal is © The Royal Society of Chemistry 2023

45 m^2 g^{-1}, 2.15 nm [Fig. 2(b)], and 0.16 cm^3 g^{-1}, respectively. In summary, Py-DSDA-COP showed significant mesoporous characteristics. The SEM images of Py-DSDA-COP revealed a nanorod-like structure with aggregated particles [Fig. 3(a) and (b)], which was also validated by TEM analysis (Fig. 3(c) and (d)) with porous characteristics.

Scheme 2 outlines the process for creating Py-DSDA-COP/ nanocomposite materials using π–π stacking interactions between Py-DSDA-COP and C60, MWCNTs, or SWCNTs. The process involves placing the Py-DSDA-COP and the chosen nanomaterial into a THF solution and sonicating the mixture overnight. This results in the formation of Py-DSDA-COP/C60, Py-DSDA-COP/MWCNTs, or Py-DSDA-COP/SWCNTs nanocomposites, respectively. TEM images of SWCNTs, MWCNTs, and fullerene (C60) and Py-DSDA-COP nanocomposites (Py-DSDA-COP/SWCNTs, Py-DSDA-COP/MWCNTs, Py-DSDA-COP/C60) are shown in (Fig. 4(a–f)). The SWCNTs and MWCNTs were observed as nanotube-like structures, while C60 has a circular shape. The SWCNTs and MWCNTs dispersed very uniformly in Py-DSDA-COP due to excellent π–π stacking interactions between them [Fig. 4(d) and (e)]. But in the case of

C60, poor dispersion was observed with Py-DSDA-COP suggesting no interaction between them (Fig. 4(f)).

Electrochemical performance of Py-DSDA-COP and its nanocomposites with C60, MWCNTs, and SWCNTs

The electrochemical performance of C60, MWCNTs, SWCNTs, Py-DSDA-COP, Py-DSDA-COP/C60, Py-DSDA-COP/MWCNTs, and Py-DSDA-COP/SWCNTs nanocomposites was measured by performing cyclic voltammetry (CV) and galvanostatic charge–discharge (GCD) analysis through a three-electrode system (1 M KOH solution). The CV curves of all Py-DSDA-COPs samples were measured at various sweep rates (5 to 200 mV s^{-1}) corresponding to the potential window between 0 and −1 V, as shown in Fig. 5(a–d) and S5(a–c).† The CV curves for MWCNTs and SWCNTs exhibited quasi-rectangular shapes with humps, indicating the presence of electric double-layer capacitance (EDLC) and pseudocapacitive responses.

In contrast, C60 displayed oxidation and reduction peaks with humps, showcasing a more pronounced pseudocapacitive nature along with EDLC.[59,60] Notably, the CV-integrated area for SWCNTs was significantly larger than that observed for
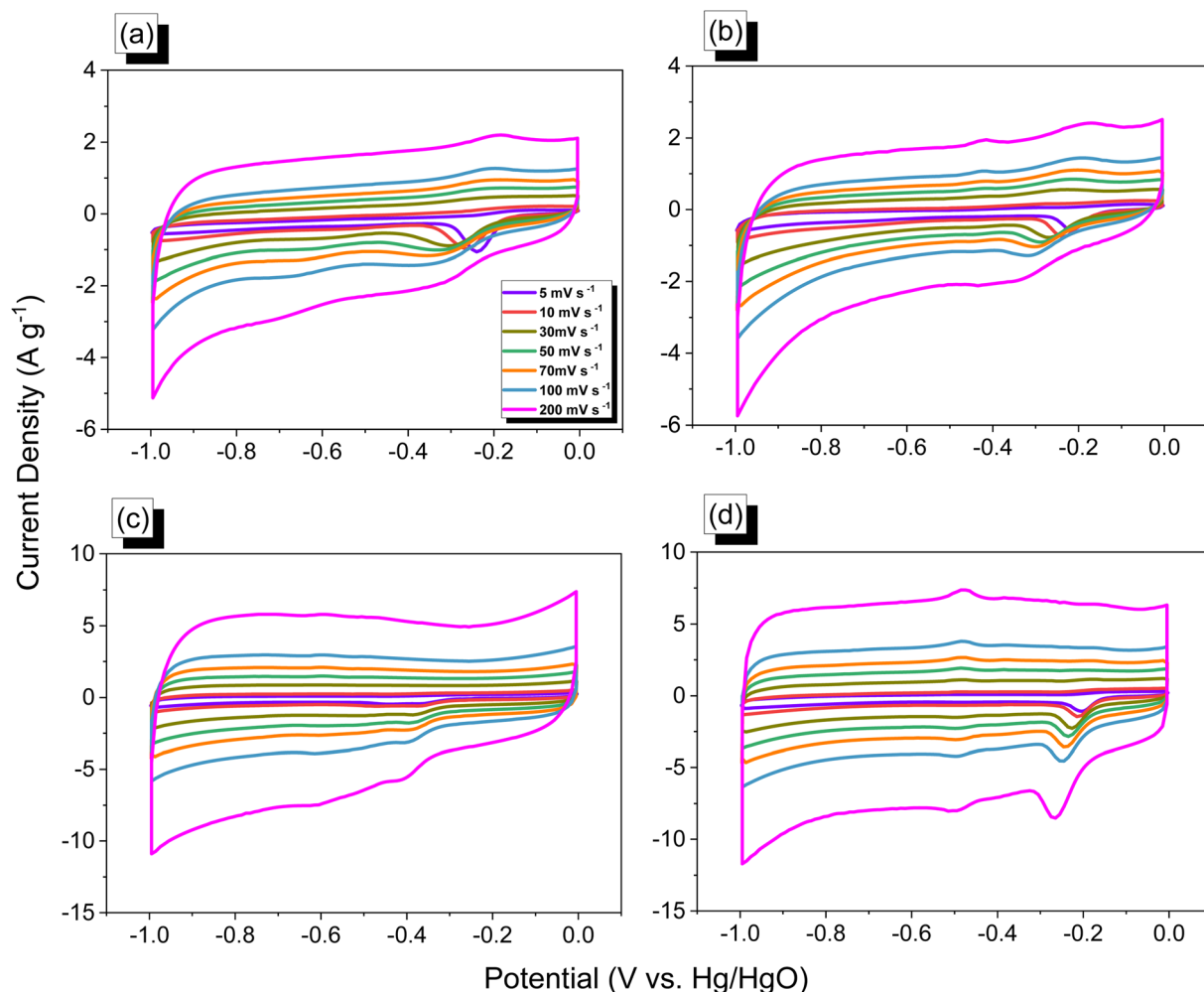

Fig. 5 CV curves of (a) Py-DSDA-COP, (b) Py-DSDA-COP/C60, (c) Py-DSDA-COP/MWCNTs and (d) Py-DSDA-COP/SWCNTs.

MWCNTs and C60, as illustrated in Fig. S5(a–c).† The CV curves of Py-DSDA-COP, Py-DSDA-COP/C60, Py-DSDA-COP/MWCNTs, and Py-DSDA-COP/SWCNTs nanocomposites showed quasi-rectangular curves with humps, revealing that the capacitive feedback was influenced by the EDLC.[59,60] The presence of humps suggests that faradaic redox currents induced another minor pseudocapacitance effect, due to the blending of nano carbonaceous materials and sulfur species (heteroatom influence) in these Py-DSDA-COPs electrodes.[55,56] The CV curves of all Py-DSDA-COP electrode samples have redox peaks, corresponding to the pseudocapacitance nature, the presence of the conjugated system, and N and S atoms in the pure Py-DSDA-COP.[55,56] Furthermore, with increasing sweep rates, current density also increased without affecting CV profiles, suggesting high-rate capability.[55,56] The CV-integrated area of Py-DSDA-COP/MWCNTs and Py-DSDA-COP/SWCNTs nanocomposites improved as compared to pure Py-DSDA-COP, indicating their higher specific capacitance. The GCD curves of Py-DSDA-COP and its nanocomposite samples were recorded at various current densities from 1 to 20 A g^{-1}, as shown in Fig. 6(a–d) and S5(d–f).† The GCD curves of C60, MWCNTs, and SWCNTs are triangular with slight bends revealing EDLC and pseudocapacitive behavior.†[59,60] The specific capacitance of C60, MWCNTs, and SWCNTs at 1 A g^{-1} was 9.8 F g^{-1}, 31.75 F g^{-1}, and 73.42 F g^{-1} respectively. The SWCNTs showed higher electrochemical performance than C60 and MWCNTs. These GCD curves of Py-DSDA-COP, Py-DSDA-COP/C60, Py-DSDA-COP/MWCNTs, and Py-DSDA-COP/SWCNTs nanocomposites have triangular shapes with a slight bend, demonstrating both pseudocapacitive and EDLC characteristics.[59,60] The Py-DSDA-COP nanocomposites (Py-DSDA-COP/C60, Py-DSDA-COP/MWCNTs, and Py-DSDA-COP/SWCNTs) experienced a higher discharging time curve than those of pure Py-DSDA-COP, revealing that after blending of different nanoparticles (C60, MWCNTs, SWCNTs), the specific capacitance of Py-DSDA-COP was improved. The specific capacitance from GCD curves at 1 A g^{-1} was observed as 56 F g^{-1}, 61 F g^{-1}, 123 F g^{-1}, and 171 F g^{-1} for Py-DSDA-COP, Py-DSDA-COP/C60, Py-DSDA-COP/MWCNTs, and Py-DSDA-COP/SWCNTs nanocomposites, respectively (Fig. 7(a)). The Py-DSDA-COP/SWCNTs showed higher specific capacitance than Py-DSDA-COP/MWCNTs, possibly due to the higher EDLC behavior, higher conductivity, and lower diameter of SWCNTs than those of MWCNTs and C60.[61,62] In addition, based on TEM images, the successful
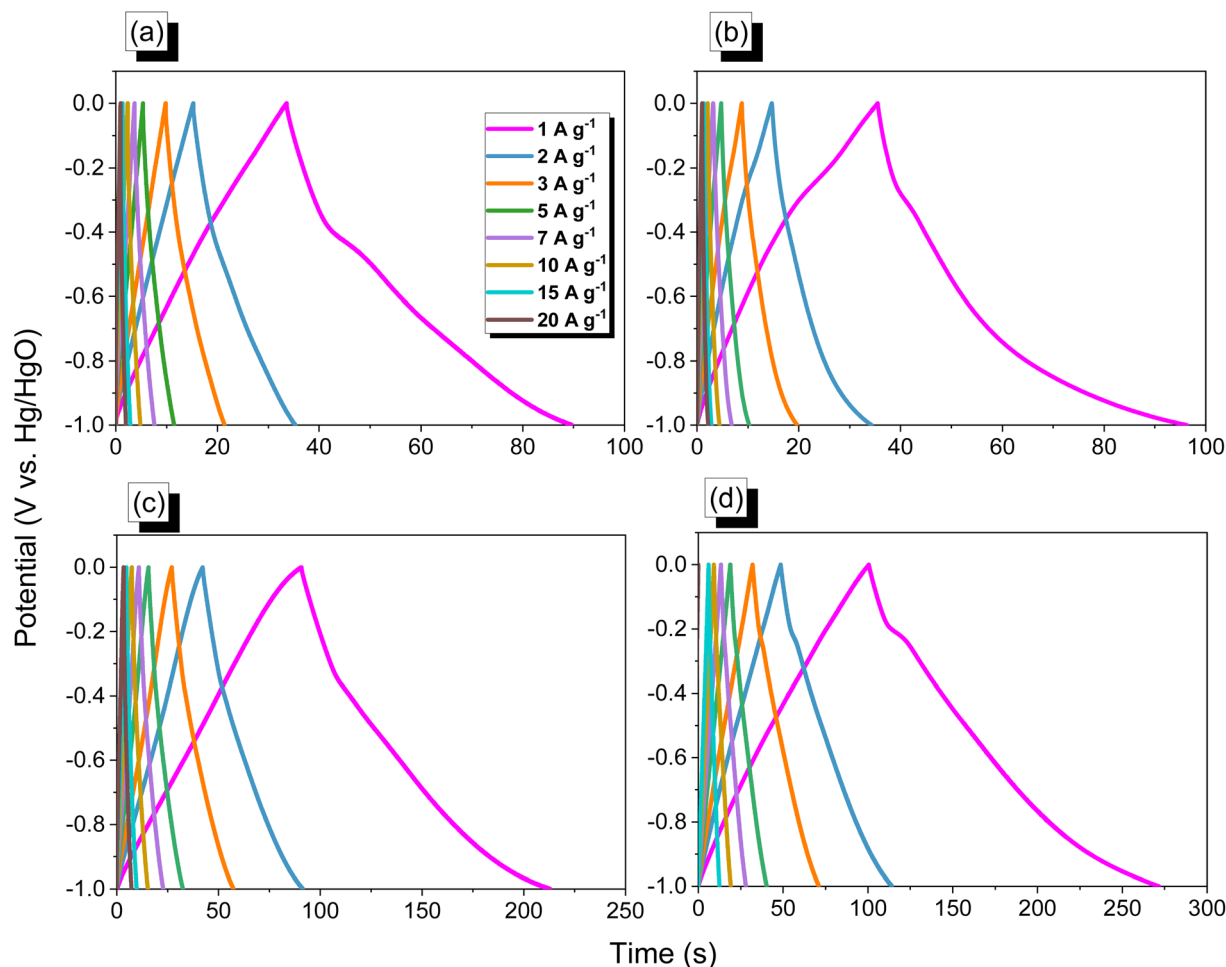

Fig. 6   GCD curves of (a) Py-DSDA-COP, (b) Py-DSDA-COP/C60, (c) Py-DSDA-COP/MWCNTs and (d) Py-DSDA-COP/SWCNTs.

22874 | J. Mater. Chem. A, 2023, 11, 22868–22883

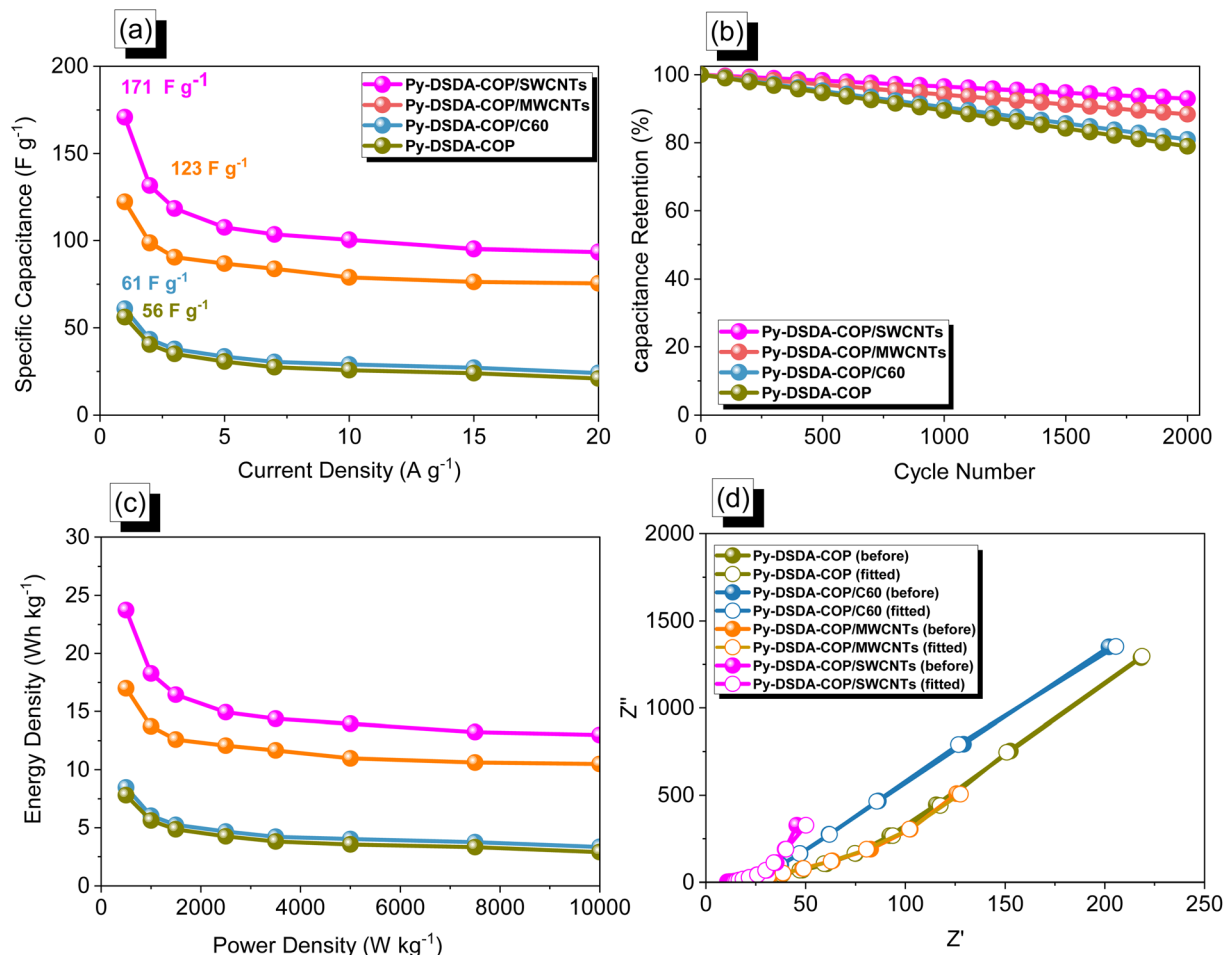This journal is © The Royal Society of Chemistry 2023

Fig. 7 (a) Specific capacity, (b) stability, (c) Ragone profiles, and (d) Nyquist plots for Py-DSDA-COP, Py-DSDA-COP/C60, Py-DSDA-COP/MWCNTs, and Py-DSDA-COP/SWCNTs.

dispersion of Py-DSDA-COP within SWCNTs results in enhanced ion mobility within the nanotubes, leading to improved ion migration efficiency and an increased capacitance. Moreover, the specific capacitance of Py-DSDA-CO' didn't enhance much by incorporating C60, due to their poor interaction as discussed above in the TEM analysis. The electrochemical performance evaluation of Py-DSDA-COP, Py-DSDA-COP/C60, Py-DSDA-COP/MWCNTs, and Py-DSDA-COP/SWCNTs was conducted using three electrode systems, and this assessment was repeated three times. The specific capacitance values were determined from the GCD curves at a current density of 1 A g^{-1} and were found to be 56.18 F g^{-1} for Py-DSDA-COP, 60.96 F g^{-1} for Py-DSDA-COP/C60, 122.3 F g^{-1} for Py-DSDA-COP/MWCNTs, and 170.8 F g^{-1} for Py-DSDA-COP/SWCNTs (Fig. S6†). Numerous materials with high capacitance values, such as MWCNT@SACMP (594 F g^{-1} at 1.0 A g^{-1}),[63] pNTCDA-TPAT (217.4 F g^{-1} at 0.5 A g^{-1}),[64] PTPA@MWNT-4 (410 F g^{-1}),[65] and CNT@TFA-COF-3 (338 F g^{-1}),[66] have been reported in the literature. The stabilities of Py-DSDA-COP and their nanocomposites were also evaluated through GCD at 10 A g^{-1} over 2000 cycles (Fig. 7(b)). The

capacitance retention of Py-DSDA-COP, Py-DSDA-COP/C60, Py-DSDA-COP/MWCNTs, and Py-DSDA-COP/SWCNTs nanocomposites was observed as 79%, 81%, 88%, and 93%, respectively, demonstrating the high stability of Py-DSDA-COP/MWCNTs. This revealed that the stability of Py-DSDA-COP improved after blending with C60, MWCNTs, and SWCNTs. The nanorod-like structure of Py-DSDA-COP remained intact, even after undergoing 2000 cycles at a rate of 10 A g^{-1}, as illustrated in Fig. S7.† We also display the Ragone plot (Fig. 7(c)), by calculating energy and power density [eqn (S2)†]. The energy density of the Py-DSDA-COP/SWCNTs nanocomposite (23.7 W h kg^{-1}) is much higher than those of Py-DSDA-COP/MWCNTs (16.9 W h kg^{-1}), Py-DSDA-COP/C60 (8.4 W h kg^{-1}) and Py-DSDA-COP (28 W h kg^{-1}). Furthermore, the internal resistance of these electrode materials was also investigated by electrochemical impedance spectroscopy (EIS). The fitted Nyquist plots (Fig. 7(d)) were used to determine series resistance (R_s) from an equivalent circuit (Fig. S8†). The series resistance was observed as 10.78, 11.02, 13.6, and 6.6 Ω for Py-DSDA-COP, Py-DSDA-COP/C60, Py-DSDA-COP/MWCNTs, and Py-DSDA-COP/SWCNTs nanocomposites, respectively. The

Py-DSDA-COP/SWCNTs displayed the smallest resistance and hence had superior electrochemical performance to the other three COP electrode materials. The blending of different carbonaceous materials in Py-DSDA-COP resulted in excellent electrochemical performance compared to other porous materials (Table S1†).

Electrochemical performance of symmetric coin cells based on Py-DSDA-COP and its nanocomposites with C60, MWCNTs, and SWCNTs

The electrochemical performance of Py-DSDA-COP and its nanocomposites were also investigated by preparing symmetric CR2032 coin cells at various sweep rates (5 to 200 mV s^{-1}) corresponding to the potential window between 0.4 and −0.6, as shown in Fig. 8. All CV curves showed quasi-rectangular curves with humps demonstrating EDLC and pseudocapacitance effect

(Fig. 8(a–d)).[55,56] The GCD curves of all electrode materials are triangular with bend-assisted EDLC and pseudocapacitance characteristics (Fig. 9(a–d)). The specific capacitance from GCD curves at 1 A g^{-1} was observed as 17 F g^{-1}, 19 F g^{-1}, 54 F g^{-1}, and 79 F g^{-1} for Py-DSDA-COP, Py-DSDA-COP/C60, Py-DSDA-COP/MWCNTs, and Py-DSDA-COP/SWCNTs nanocomposites respectively (Fig. 10(a)). The incorporation of SWCNTs into Py-DSDA-COP led to higher specific capacitance due to their good dispersion, higher EDLC behavior, higher conductivity, and lower diameter than those of MWCNTs, while C60 showed poor dispersion in Py-DSDA-COP, revealing no interaction between them. The stability of Py-DSDA-COP and its nanocomposites were also evaluated through GCD at 10 A g^{-1} over 2000 cycles for symmetric coin cells (Fig. 10(b)), showing a capacitance retention of 95%, 89.4%, 80.6%, and 78.4% for Py-DSDA-COP/SWCNTs, Py-DSDA-COP/MWCNTs, Py-DSDA-COP/C60, and Py-DSDA-COP, respectively.
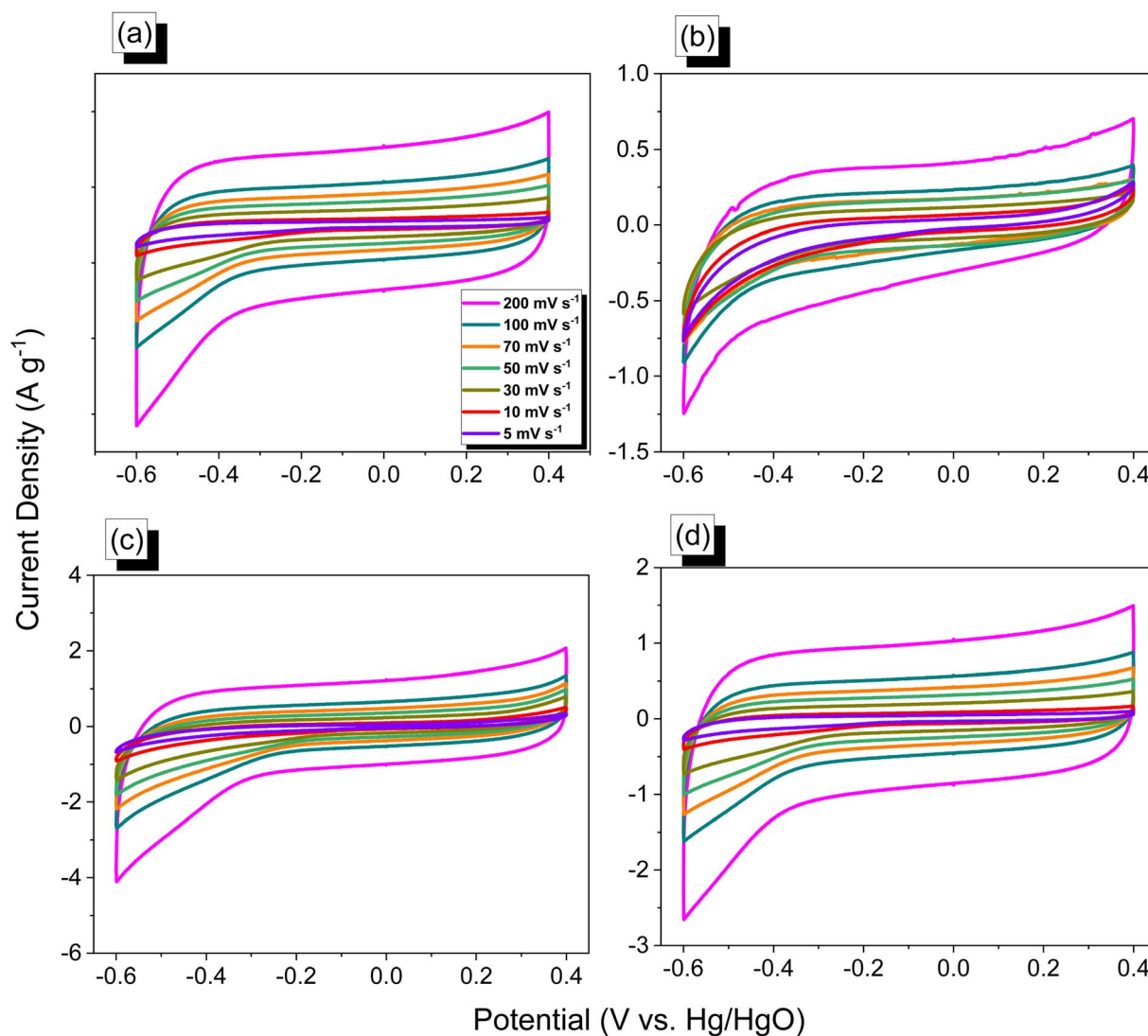

Fig. 8 CV curves of symmetric coin cells based on (a) Py-DSDA-COP, (b) Py-DSDA-COP/C60, (c) Py-DSDA-COP/MWCNTs and (d) Py-DSDA-COP/SWCNTs.
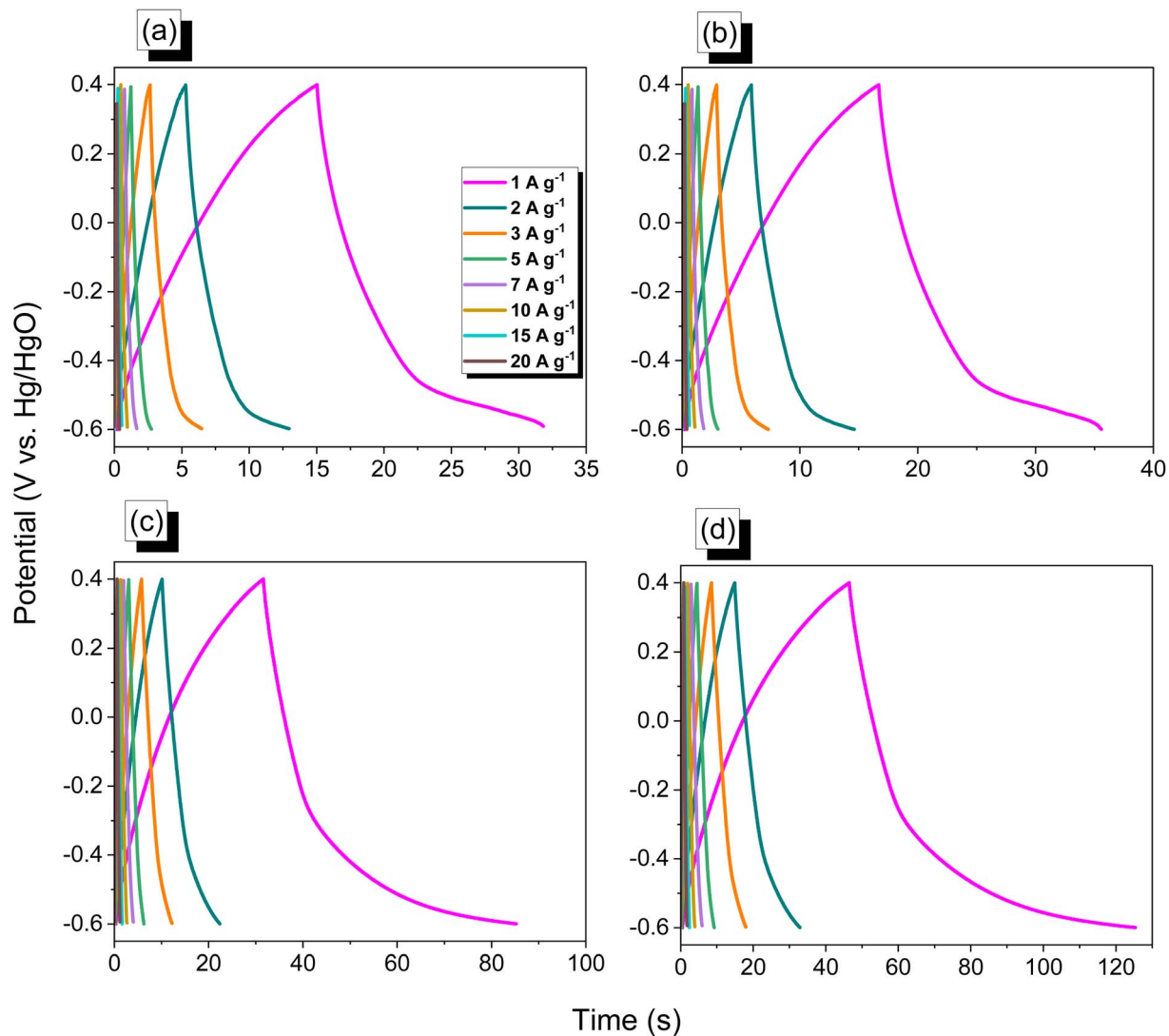
22876 | J. Mater. Chem. A, 2023, 11, 22868–22883

This journal is © The Royal Society of Chemistry 2023

Fig. 9 GCD curves of symmetric coin cells based on (a) Py-DSDA-COP, (b) Py-DSDA-COP/C60, (c) Py-DSDA-COP/MWCNTs and (d) Py-DSDA-COP/SWCNTs.
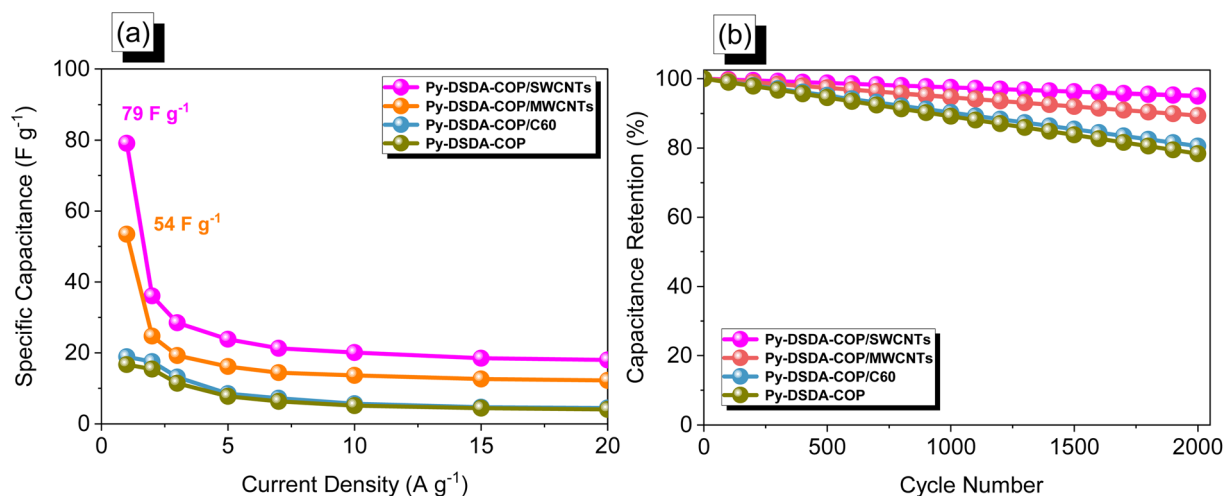
Fig. 10 (a) Specific capacity and (b) stability of symmetric coin cells based on Py-DSDA-COP, Py-DSDA-COP/C60, Py-DSDA-COP/MWCNTs, and Py-DSDA-COP/SWCNTs.
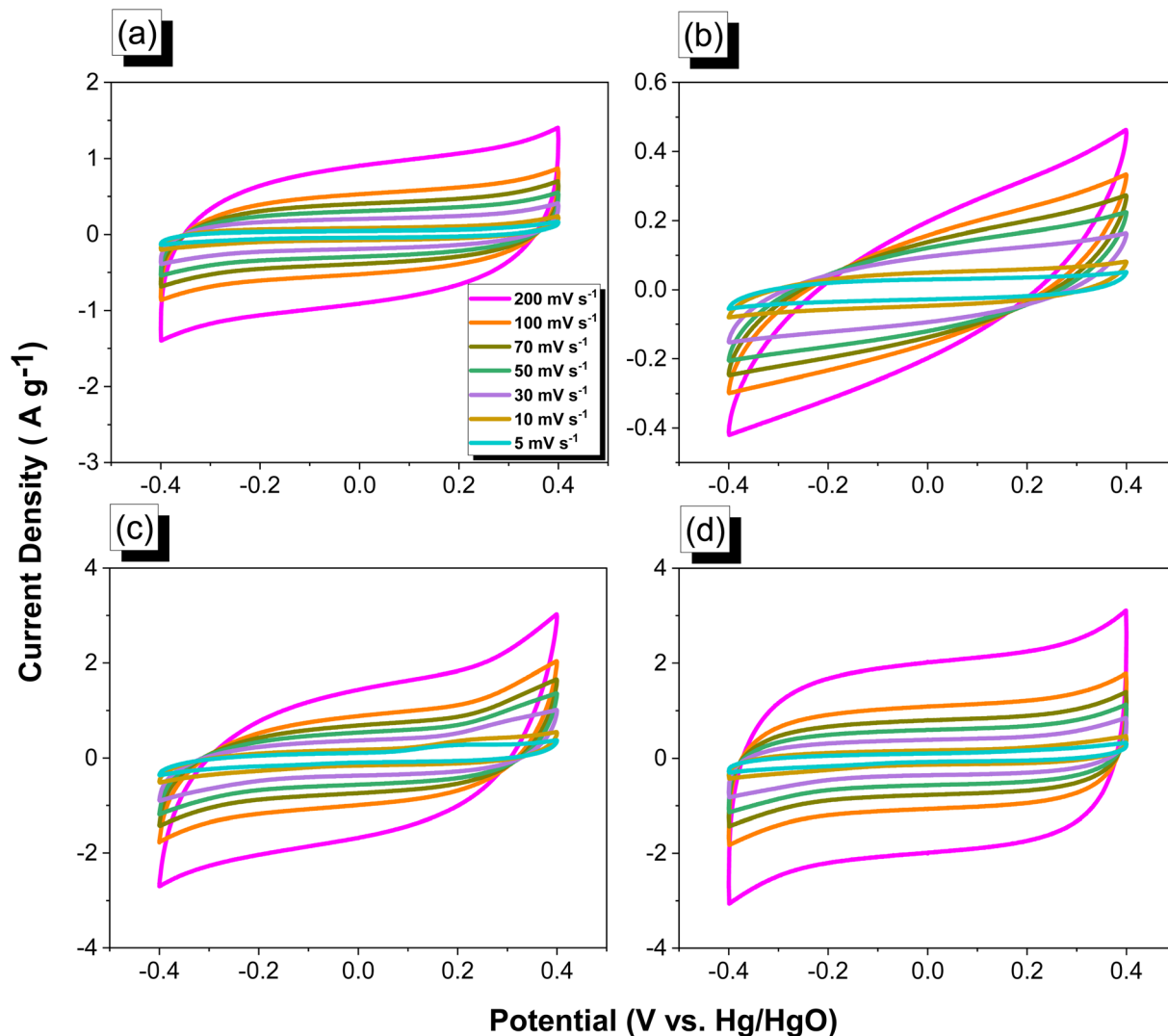
This journal is © The Royal Society of Chemistry 2023

J. Mater. Chem. A, 2023, **11**, 22868–22883 | **22877**

Fig. 11 CV curves of asymmetric coin cells based on (a) Py-DSDA-COP, (b) Py-DSDA-COP/C60, (c) Py-DSDA-COP/MWCNTs and (d) Py-DSDA-COP/SWCNTs.

Electrochemical performance of asymmetric coin cells based on Py-DSDA-COP and its nanocomposites with C60, MWCNTs, and SWCNTs

We conducted experiments involving asymmetric coin cells using Py-DSDA-COP and its nanocomposites to examine their electrochemical performance. In these coin cells, activated carbon served as the negative electrode, while Py-DSDA-COP or its nanocomposites acted as the positive electrode. We conducted tests at various sweep rates, ranging from 5 to 200 mV s^{-1}, within a potential window spanning from 0.4 to −0.4 V, as illustrated in Fig. 11. The CV curves for Py-DSDA-COP, Py-DSDA-COP/MWCNTs, Py-DSDA-COP/SWCNTs, and Py-DSDA-COP/C60 exhibited nearly rectangular shapes with slight humps, as depicted in Fig. 11(a–d). However, Py-DSDA-COP/C60 displayed a non-rectangular shape. These variations in CV curve shapes were primarily due to differences in potential windows when compared to three-electrode and symmetric coin cells. GCD

analysis showed that all electrode materials exhibited triangular curves with bends, indicating a combination of EDLC and pseudocapacitance characteristics, as shown in Fig. 12(a–d). Specific capacitance measurements at 1 A g^{-1} revealed values of 30.52 F g^{-1} for Py-DSDA-COP, 36.57 F g^{-1} for Py-DSDA-COP/C60, 79.21 F g^{-1} for Py-DSDA-COP/MWCNTs, and 113.17 F g^{-1} for Py-DSDA-COP/SWCNTs nanocomposites, as demonstrated in Fig. 13(a). Notably, Py-DSDA-COP/SWCNTs exhibited the highest specific capacitance among the prepared nanocomposite electrode materials, consistent with the results obtained using three-electrode and symmetric coin cell configurations. To assess the stability of these electrode materials, we subjected them to 10 A g^{-1} cycling for 2000 cycles in asymmetric coin cells, as shown in Fig. 13(b). The capacitance retention percentages for Py-DSDA-COP, Py-DSDA-COP/C60, Py-DSDA-COP/MWCNTs, and Py-DSDA-COP/SWCNTs nanocomposites were 78%, 82%, 88%, and 95%, respectively.
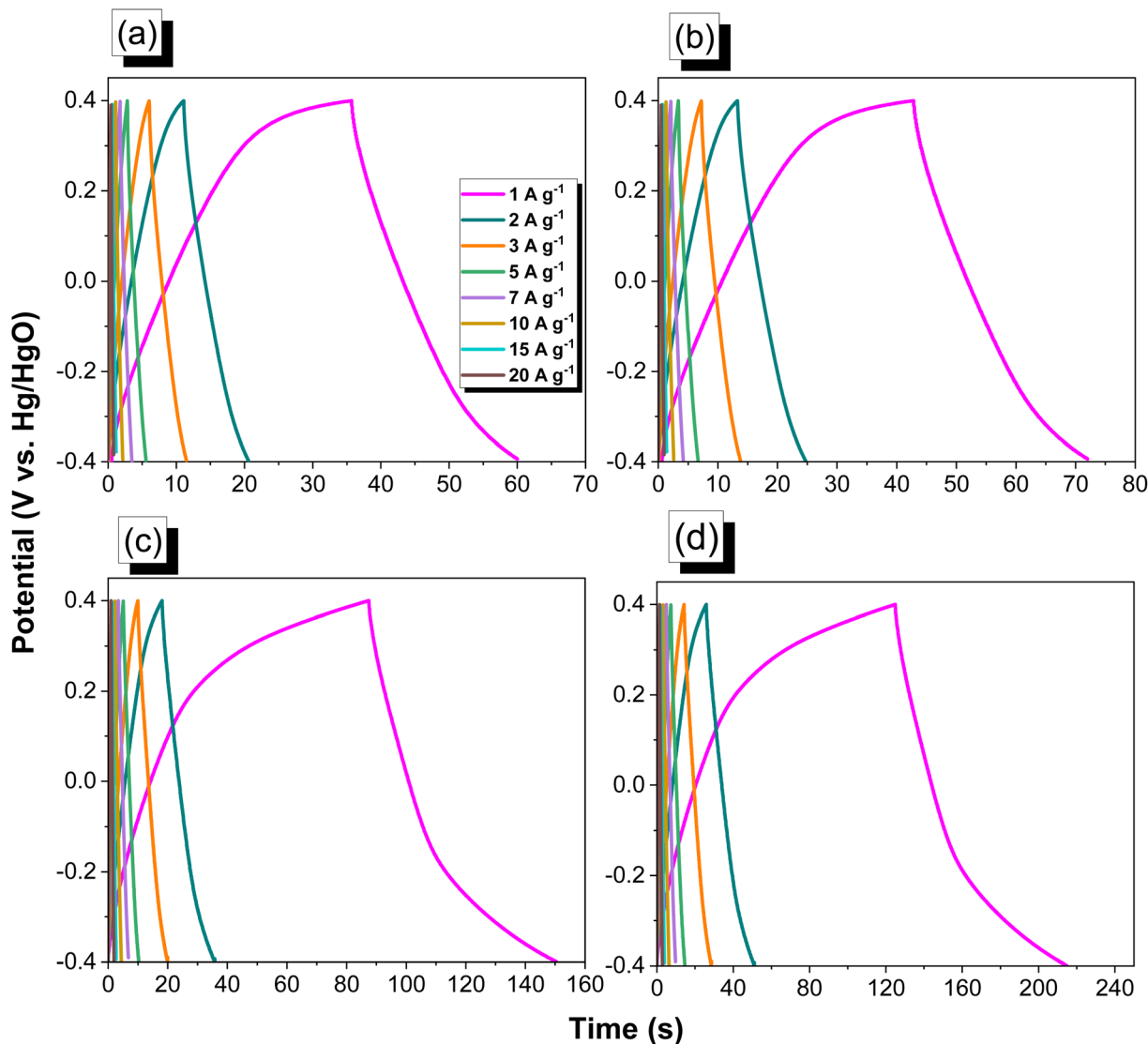
22878 | *J. Mater. Chem. A*, 2023, **11**, 22868–22883

This journal is © The Royal Society of Chemistry 2023

Fig. 12 GCD curves of asymmetric coin cells based on (a) Py-DSDA-COP, (b) Py-DSDA-COP/C60, (c) Py-DSDA-COP/MWCNTs and (d) Py-DSDA-COP/SWCNTs.
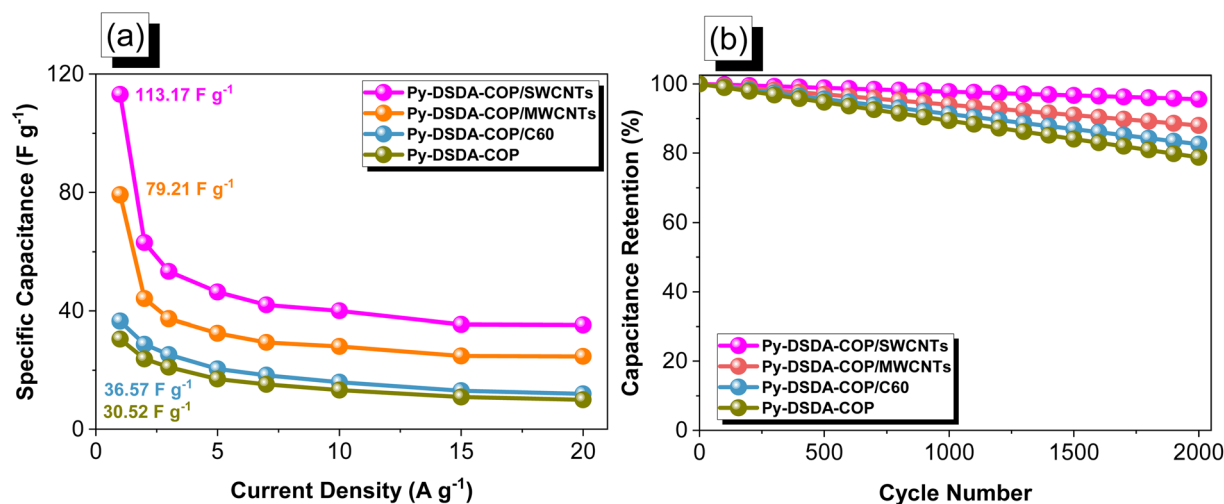

Fig. 13 (a) Specific capacity and (b) stability of asymmetric coin cells based on Py-DSDA-COP, Py-DSDA-COP, Py-DSDA-COP/MWCNTs, and Py-DSDA-COP/SWCNTs.

Conclusion

We used the Schiff base reaction to synthesize Py-DSDA-COP and investigate it as an electrode material for supercapacitors, demonstrating good porosity and a specific capacitance of 56.18 F g^{-1} at 1 A g^{-1}. We incorporated different carbonaceous materials into Py-DSDA-COP to afford Py-DSDA-COP/SWCNTs, Py-DSDA-COP/MWCNTs, and Py-DSDA-COP/C60 nano-composites to improve and compare the electrochemical performance of these electrode materials. The Py-DSDA-COP/SWCNTs displayed superior specific capacitance (171 F g^{-1}) at 1 A g^{-1} and higher energy density (23.7 W h kg^{-1}) with a capacity retention of 93% after 2000 cycles than those of Py-DSDA-COP/MWCNTs (123 F g^{-1}) and Py-DSDA-COP/C60 (61 F g^{-1}) for three electrode configurations. For symmetric coin cells, the specific capacitance was observed as 79, 54, 19, and 17 F g^{-1} for Py-DSDA-COP, Py-DSDA-COP/C60, Py-DSDA-COP/MWCNTs, and Py-DSDA-COP/SWCNTs nanocomposites, respectively. For asymmetric coin cells, the specific capacitance was observed as 30.52, 36.57, 79.21, and 113.17 F g^{-1} for Py-DSDA-COP, Py-DSDA-COP/C60, Py-DSDA-COP/MWCNTs, and Py-DSDA-COP/SWCNTs nanocomposites, respectively. The superior electrochemical properties of Py-DSDA-COP/SWCNTs are attributed to the good dispersion, higher EDLC behavior, higher conductivity, and lower diameter of SWCNTs compared to MWCNTs, while C60 doesn't show any compatibility with Py-DSDA-COP.

Conflicts of interest

There are no conflicts to declare.

Acknowledgements

Notes and references

1   Z. Xiang, D. Cao and L. Dai, Well-defined two dimensional covalent organic polymers: rational design, controlled syntheses, and potential applications, *Polym. Chem.*, 2015, **6**, 1896–1911, DOI: **10.1039/C4PY01383B**.

2   X. Guan, Y. Zhao, H. Pei, M. Zhao, Y. Wang, X. Zhou, M. G. Mohamed, S. W. Kuo and Y. Ye, Metalloporphyrin conjugated porous polymer in-situ grown on a Celgard separator as multifunctional polysulfide barrier and catalyst for high-performance Li-S batteries, *Chem. Eng. J.*, 2023, **473**, 144733, DOI: **10.1016/j.cej.2023.144733**.

3   A. O. Mousa, M. G. Mohamed, C. H. Chuang and S. W. Kuo, Carbonized Aminal-Linked Porous Organic Polymers Containing Pyrene and Triazine Units for Gas Uptake and Energy Storage, *Polymers*, 2023, **15**, 1891, DOI: **10.3390/polym15081891**.

4   T. Skorjanc, D. Shetty and A. Trabolsi, Pollutant removal with organic macrocycle-based covalent organic polymers and frameworks, *Chem*, 2021, **7**, 882–918, DOI: **10.1016/j.chempr.2021.01.002**.

5   A. O. Mousa, Z. I. Lin, C. H. Chuang, C. K. Chen, S. W. Kuo and M. G. Mohamed, Rational Design of Bifunctional Microporous Organic Polymers Containing Anthracene and Triphenylamine Units for Energy Storage and Biological Applications, *Int. J. Mol. Sci.*, 2023, **24**, 8966, DOI: **10.3390/ijms24108966**.

6   M. Ejaz, M. G. Mohamed and S. W. Kuo, Solid state chemical transformation provides a fully benzoxazine-linked porous organic polymer displaying enhanced CO_2 capture and supercapacitor performance, *Polym. Chem.*, 2023, **14**, 2494–2509, DOI: **10.1039/D3PY00158J**.

7   B. C. Patra, S. Khilari, R. N. Manna, S. Mondal, D. Pradhan, A. Pradhan and A. Bhaumik, A metal-free covalent organic polymer for electrocatalytic hydrogen evolution, *ACS Catal.*, 2017, **7**, 6120–6127, DOI: **10.1021/acscatal.7b01067**.

8   F. Alduraiei, S. Kumar, J. Liu, S. P. Nunes and G. Szekely, Rapid fabrication of fluorinated covalent organic polymer membranes for organic solvent nanofiltration, *J. Membr. Sci.*, 2022, **648**, 120345, DOI: **10.1016/j.memsci.2022.120345**.

9   K. Geng, T. He, R. Liu, S. Dalapati, K. T. Tan, Z. Li and D. Jiang, Covalent organic frameworks: design, synthesis, and functions, *Chem. Rev.*, 2020, **120**, 8814–8933, DOI: **10.1021/acs.chemrev.9b00550**.

10   D. Tao, L. Feng, Y. Chao, C. Liang, X. Song, H. Wang, K. Yang and Z. Liu, Covalent organic polymers based on fluorinated porphyrin as oxygen nanoshuttles for tumor hypoxia relief and enhanced photodynamic therapy, *Adv. Funct. Mater.*, 2018, **28**, 1804901, DOI: **10.1002/adfm.201804901**.

11   H. Shin, D. Kim, H. J. Kim, J. Kim, K. Char, C. T. Yavuz and J. W. Choi, Fluorinated covalent organic polymers for high performance sulfur cathodes in lithium–sulfur batteries, *Chem. Mater.*, 2019, **31**, 7910–7921, DOI: **10.1021/acs.chemmater.9b01986**.

12   X. Li, Q. Liu, B. Yang, Z. Liao, W. Yan and Z. Xiang, An Initial Covalent Organic Polymer with Closed-F Edges Directly for Proton-Exchange-Membrane Fuel Cells, *Adv. Mater.*, 2022, **34**, 2204570, DOI: **10.1002/adma.202204570**.

13   M. G. Mohamed, A. M. Elewa, M. S. Li and S. W. Kuo, Construction and multifunctional of hypercrosslinked porous organic polymers containing ferrocene unit for high-performance iodine adsorption and supercapacitor, *J. Taiwan Inst. Chem. Eng.*, 2023, **150**, 105045, DOI: **10.1016/j.jtice.2023.105045**.

14   A. O. Mousa, C. H. Chuang, S. W. Kuo and M. G. Mohamed, Strategic Design and Synthesis of Ferrocene Linked Porous Organic Frameworks toward Tunable CO_2 Capture and Energy Storage, *Int. J. Mol. Sci.*, 2023, **24**, 12371, DOI: **10.3390/ijms241512371**.

15   M. G. Mohamed, H. Y. Hu, M. Madhu, M. M. Samy, I. M. A. Mekhemer, W. L. Tseng, H. H. Chou and S. W. Kuo, Ultrastable two-dimensional fluorescent conjugated microporous polymers containing pyrene and fluorene units for metal ion sensing and energy storage,

22880 | *J. Mater. Chem. A*, 2023, **11**, 22868–22883

This journal is © The Royal Society of Chemistry 2023

Eur. Polym. J., 2023, **189**, 111980, DOI: **10.1016/j.eurpolymj.2023.111980**.

16 K. Prakash and D. T. Masram, Chromogenic covalent organic polymer-based microspheres as solid-state gas sensor, *J. Mater. Chem. C*, 2020, **8**, 9201–9204, DOI: **10.1039/D0TC02129F**.

17 N. Nouruzi, M. Dinari, B. Gholipour, N. Mokhtari, M. Farajzadeh, S. Rostamnia and M. Shokouhimehr, Photocatalytic hydrogen generation using colloidal covalent organic polymers decorated bimetallic Au-Pd nanoalloy (COPs/Pd-Au), *Mol. Catal.*, 2022, **518**, 112058, DOI: **10.1016/j.mcat.2021.112058**.

18 A. Wang, A. L. Cheng, W. Zhao, X. Shen and W. Zhu, Electrochemical hydrogen and oxygen evolution reactions from a cobalt-porphyrin-based covalent organic polymer, *J. Colloid Interface Sci.*, 2020, **579**, 598–606, DOI: **10.1016/j.jcis.2020.06.109**.

19 N. Sang, C. Zhan and D. Cao, Highly sensitive and selective detection of 2, 4, 6-trinitrophenol using covalent-organic polymer luminescent probes, *J. Mater. Chem. A*, 2015, **3**, 92–96, DOI: **10.1039/C4TA04903A**.

20 Z. Yang, D. Tao, W. Zhong, Z. Liu, L. Feng and M. Chen, Perfluorocarbon loaded fluorinated covalent organic polymers with effective sonosensitization and tumor hypoxia relief enable synergistic sonodynamic-immunotherapy, *Biomaterials*, 2022, **280**, 121250, DOI: **10.1016/j.biomaterials.2021.121250**.

21 S. Ravi, P. Puthiaraj, K. Yu and W. S. Ahn, Porous covalent organic polymers comprising a phosphite skeleton for aqueous Nd (III) capture, *ACS Appl. Mater. Interfaces*, 2019, **11**, 11488–11497, DOI: **10.1021/acsami.9b00546**.

22 W. Zhang, Y. Liu, Y. Luo, C. Xie, Z. Xiang and J. F. Chen, HiGee strategy toward rapid mass production of porous covalent organic polymers with superior methane deliverable capacity, *Adv. Funct. Mater.*, 2020, **30**, 1908079, DOI: **10.1002/adfm.201908079**.

23 I. Ahmed, H. J. Lee and S. H. Jhung, Covalent-organic polymer-derived carbons: An effective adsorbent to remove sulfonamide antibiotics from water, *Chem. Eng. J.*, 2022, **437**, 135386, DOI: **10.1016/j.cej.2022.135386**.

24 M. Wang, L. Guo and L. D. Cao, Covalent organic polymers for rapid fluorescence imaging of latent fingerprints, *ACS Appl. Mater. Interfaces*, 2018, **10**, 21619–21627, DOI: **10.1021/acsami.8b05213**.

25 Q. Yang, P. Peng and Z. Xiang, Covalent organic polymer modified TiO_2 nanosheets as highly efficient photocatalysts for hydrogen generation, *Chem. Eng. Sci.*, 2017, **162**, 33–40, DOI: **10.1016/j.ces.2016.12.071**.

26 Z. Xiang, D. Cao, W. Wang, W. Yang, B. Han and J. Lu, Postsynthetic lithium modification of covalent-organic polymers for enhancing hydrogen and carbon dioxide storage. The J, *J. Phys. Chem. C*, 2012, **116**, 5974–5980, DOI: **10.1021/jp300137e**.

27 S. Y. Chang, A. M. Elewa, M. G. Mohamed, I. M. A. Mekhemer, M. M. Samy, K. Zhang, H. H. Chou and S. W. Kuo, Rational design and synthesis of bifunctional Dibenzo[g,p]chrysene-based conjugated microporous polymers for energy storage and visible light-driven photocatalytic hydrogen evolution, *Mater. Today Chem.*, 2023, **33**, 101680, DOI: **10.1016/j.mtchem.2023.101680**.

28 M. G. Mohamed, S. Y. Chang, M. Ejaz, M. M. Samy, A. O. Mousa and S. W. Kuo, Design and Synthesis of Bisulfone-Linked Two-Dimensional Conjugated Microporous Polymers for CO_2 Adsorption and Energy Storage, *Molecules*, 2023, **28**, 3234, DOI: **10.3390/molecules28073234**.

29 J. Wei, D. Wang, J. Li, J. Zhang, N. Wang and J. Li, A benzimidazole-linked porphyrin covalent organic polymers as efficient heterogeneous catalyst/photocatalyst, *Appl. Organomet. Chem.*, 2022, **36**, e6820, DOI: **10.1002/aoc.6820**.

30 D. Yadav and S. K. Awasthi, A Pd NP-confined novel covalent organic polymer for catalytic applications, *New J. Chem.*, 2020, **44**, 1320–1325, DOI: **10.1039/C9NJ05827C**.

31 V. Sadhasivam, M. Harikrishnan, G. Elamathi, R. Balasaravanan, S. Murugesan and A. Siva, Copper nanoparticles supported on highly nitrogen-rich covalent organic polymers as heterogeneous catalysts for the ipso-hydroxylation of phenyl boronic acid to phenol, *New J. Chem.*, 2020, **44**, 6222–6231, DOI: **10.1039/C9NJ05759E**.

32 Y. Wang, H. Ji, X. Zhang, J. Shi, X. Li, X. Jiang and X. Qu, Cyclopropenium cationic-based covalent organic polymer-enhanced poly (ethylene oxide) composite polymer electrolyte for all-solid-state Li–S battery, *ACS Appl. Mater. Interfaces*, 2021, **13**, 16469–16477, DOI: **10.1021/acsami.1c02309**.

33 X. Liu, C. F. Liu, W. Y. Lai and W. Huang, Porous organic polymers as promising electrode materials for energy storage devices, *Adv. Mater. Technol.*, 2020, **5**, 2000154, DOI: **10.1002/admt.202000154**.

34 M. Gao, M. J. Zheng, A. F. M. EL-Mahdy, C. W. Chang, Y. C. Su, W. H. Hung, S. W. Kuo and L. H. Yeh, A bioinspired ionic diode membrane based on sub-2 nm covalent organic framework channels for ultrahigh osmotic energy generation, *Nano Energy*, 2023, **105**, 108007, DOI: **10.1016/j.nanoen.2022.108007**.

35 M. G. Mohamed, S. V. Chaganti, M. S. Li, M. M. Samy, S. U. Sharma, J. T. Lee, M. H. Elsayed and S. W. Kuo, Ultrastable Porous Organic Polymers Containing Thianthrene and Pyrene Units as Organic Electrode Materials for Supercapacitors, *ACS Appl. Energy Mater.*, 2022, **5**, 6442–6452, DOI: **10.1021/acsaem.2c00942**.

36 K. Sharma, A. Arora and S. K. Tripathi, Review of supercapacitors: Materials and devices, *J. Energy Storage*, 2019, **21**, 801–825, DOI: **10.1016/j.est.2019.01.010**.

37 D. P. Chatterjee and A. K. Nandi, A review on the recent advances in hybrid supercapacitors, *J. Mater. Chem. A*, 2021, **9**, 15880–15918, DOI: **10.1039/D1TA02505H**.

38 A. G. Olabi, Q. Abbas, A. Al Makky and M. A. Abdelkareem, Supercapacitors as next generation energy storage devices: Properties and applications, *Energy*, 2022, **248**, 123617, DOI: **10.1016/j.energy.2022.123617**.

39 T. Mao, S. Wang, X. Wang, F. Liu, J. Li, H. Chen, D. Wang, G. Liu, J. Xu and Z. Wang, High-temperature and all-solid-state flexible supercapacitors with excellent long-term

This journal is © The Royal Society of Chemistry 2023

J. Mater. Chem. A, 2023, **11**, 22868–22883 | **22881**

stability based on porous polybenzimidazole/functional ionic liquid electrolyte, *ACS Appl. Mater. Interfaces*, 2019, **11**, 17742–17750, DOI: 10.1021/acsami.9b00452.

40 L. Zheng, B. Tang, X. Dai, T. Xing, Y. Ouyang, Y. Wang, B. Chang, H. Shu and X. Wang, High-yield synthesis of N-rich polymer-derived porous carbon with nanorod-like structure and ultrahigh N-doped content for high-performance supercapacitors, *Chem. Eng. J.*, 2020, **399**, 125671, DOI: 10.1016/j.cej.2020.125671.

41 M. Ejaz, M. M. Samy, Y. Ye, S. W. Kuo and M. G. Mohamed, Design hybrid porous organic/inorganic polymers containing polyhedral oligomeric Silsesquioxane/Pyrene/Anthracene moieties as a high-performance electrode for supercapacitor, *Int. J. Mol. Sci.*, 2023, **24**, 2501, DOI: 10.3390/ijms24032501.

42 S. Kiruthika, N. Sneha and R. Gupta, Visibly transparent supercapacitors, *J. Mater. Chem. A*, 2023, **11**, 4907–4936, DOI: 10.1039/D2TA07836H.

43 M. Ejaz, M. G. Mohamed, S. U. Sharma, J. T. Lee, C. F. Huang, T. Chen and S. W. Kuo, An ultrastable porous polyhedral oligomeric silsesquioxane/tetraphenylthiophene hybrid as a high-performance electrode for supercapacitors, *Molecules*, 2022, **27**, 6238, DOI: 10.3390/molecules27196238.

44 M. M. Samy, M. G. Mohamed, S. U. Sharma, S. V. Chaganti, J. T. Lee and S. W. Kuo, An Ultrastable Tetrabenzonaphthalene-Linked conjugated microporous polymer functioning as a high-performance electrode for supercapacitors, *J. Taiwan Inst. Chem. Eng.*, 2023, 104750, DOI: 10.1016/j.jtice.2023.104750.

45 J. Huang, Y. Hu, H. Wang, T. Wang, H. Wu, J. Li, M. Wang and J. Zhang, Lignin Isolated from Poplar Wood for Porous Carbons as Electrode for High-Energy Renewable Supercapacitor Driven by Lignin/Deep Eutectic Solvent Composite Gel Polymer Electrolyte, *ACS Appl. Energy Mater.*, 2022, **5**, 6393–6400, DOI: 10.1021/acsaem.2c00835.

46 D. Hu, Y. Jia, S. Yang, F. Huang, Y. Dong and P. Du, Redox-active 2D porous organic polymers for high-performance supercapacitor, *J. Ind. Eng. Chem.*, 2023, **123**, 320–329, DOI: 10.1016/j.jiec.2023.03.049.

47 S. Wang, Y. Z. Guo, F. X. Wang, S. H. Zhou, T. Y. Zeng and Y. B. Dong, Research progress on metal and covalent organic framework-based materials for high-performance supercapacitors, *New Carbon Mater.*, 2022, **37**, 109–135, DOI: 10.1016/S1872-5805(22)60586-9.

48 M. G. Mohamed, E. C. Atayde Jr, B. M. Matsagar, J. Na, Y. Yamauchi, K. C. W. Wu and S. W. Kuo, Construction Hierarchically Mesoporous/Microporous Materials Based on Block Copolymer and Covalent Organic Framework, *J. Taiwan Inst. Chem. Eng.*, 2020, **112**, 180–192, DOI: 10.1016/j.jtice.2020.06.013.

49 D. T. Bakhoum, K. O. Oyedotun, S. Sarr, N. F. Sylla, V. M. Maphiri, N. M. Ndiaye, B. D. Ngom and N. Manyala, A study of porous carbon structures derived from composite of cross-linked polymers and reduced graphene oxide for supercapacitor applications, *J. Energy Storage*, 2022, **51**, 104476, DOI: 10.1016/j.est.2022.104476.

50 J. Tong, J. Wang, P. Xu and S. Zhang, Nitrogen and oxygen codoped porous carbon based on a synthetic polymer for high-performance solid-state supercapacitors, *J. Energy Storage*, 2023, **58**, 106349, DOI: 10.1016/j.est.2022.106349.

51 J. Zhang, H. Zhao, J. Li, H. Jin, X. Yu, Y. Lei and S. Wang, In Situ Encapsulation of Iron Complex Nanoparticles into Biomass-Derived Heteroatom-Enriched Carbon Nanotubes for High-Performance Supercapacitors, *Adv. Energy Mater.*, 2019, **9**, 1803221, DOI: 10.1002/aenm.201803221.

52 S. Deshagani, X. Liu, B. Wu and M. Deepa, Nickel Cobaltite@Poly(3,4-ethylenedioxypyrrole) and Carbon Nanofiber Interlayer Based Flexible Supercapacitor, *Nanoscale*, 2019, **11**, 2742–2756, DOI: 10.1039/C8NR08645A.

53 H. Ma, C. Li, M. Zhang, J. D. Hong and G. Shi, Graphene Oxide Induced Hydrothermal Carbonization of Egg Proteins for High Performance Supercapacitors, *J. Mater. Chem. A*, 2017, **5**, 17040–17074, DOI: 10.1039/C7TA04771A.

54 Y. Deng, Y. Xie, K. Zou and X. Ji, Review on Recent Advances in Nitrogen-Doped Carbons: Preparations and Applications in Supercapacitors, *J. Mater. Chem. A*, 2016, **4**, 1144–1173, DOI: 10.1039/C5TA08620E.

55 M. G. Mohamed, M. M. Samy, T. H. Mansoure, S. U. Sharma, M. S. Tsai, J. H. Chen, J. T. Lee and S. W. Kuo, Dispersions of 1,3,4-oxadiazole-linked conjugated microporous polymers with carbon nanotubes as a high-performance electrode for supercapacitors, *ACS Appl. Energy Mater.*, 2022, **5**, 3677–3688, DOI: 10.1021/acsaem.2c00100.

56 M. M. Samy, M. G. Mohamed, A. F. M. El-Mahdy, T. H. Mansoure, K. C. W. Wu and S. W. Kuo, High-performance supercapacitor electrodes prepared from dispersions of tetrabenzonaphthalene-based conjugated microporous polymers and carbon nanotubes, *ACS Appl. Mater. Interfaces*, 2021, **13**, 51906–51916, DOI: 10.1021/acsami.1c05720.

57 L. Mei, X. Cui, Q. Duan, Y. Li, X. Lv and H. G. Wang, Metal Phthalocyanine-Linked Conjugated Microporous Polymer Hybridized with Carbon Nanotubes as a High-Performance Flexible Electrode for Supercapacitors, *Int. J. Hydrogen Energy*, 2020, **45**, 22950–22958, DOI: 10.1016/j.ijhydene.2020.06.208.

58 Y. Zhang, B. Lin, Y. Sun, X. Zhang, H. Yang and J. Wang, Carbon Nanotubes@Metal-Organic Frameworks as Mn-Based Symmetrical Supercapacitor Electrodes for Enhanced Charge Storage, *RSC Adv.*, 2015, **5**, 58100–58106, DOI: 10.1039/C5RA11597C.

59 M. M. Samy, M. G. Mohamed and S. W. Kuo, Pyrene-functionalized tetraphenylethylene polybenzoxazine for dispersing single-walled carbon nanotubes and energy storage, *Compos. Sci. Technol.*, 2020, **199**, 108360, DOI: 10.1016/j.compscitech.2020.108360.

60 M. M. Samy, M. G. Mohamed and S. W. Kuo, Conjugated Microporous Polymers Based on Ferrocene Units as Highly Efficient Electrodes for Energy Storage, *Polymers*, 2020, **15**, 1095, DOI: 10.3390/polym15051095.

61 S. Zhou, S. Zeng, S. Zhang, J. Qiao, J. Di, M. Chen, N. Liu and Q. Li, Hierarchical carbon nanotube hybrid films for high-

performance all-solid-state supercapacitors, *RSC Adv.*, 2017, **7**, 52010–52016, DOI: **10.1039/C7RA10581A**.

62 P. Sivaraman, S. P. Mishra, D. D. Potphode, A. P. Thakur, K. Shashidhara, A. B. Samui and A. R. Bhattacharyya, A supercapacitor based on longitudinal unzipping of multi-walled carbon nanotubes for high temperature application, *RSC Adv.*, 2015, **5**, 83546–83557, DOI: **10.1039/C5RA13136G**.

63 W. Lyu, C. Yan, Z. Chen, J. Chen, H. Zuo, L. Teng, H. Liu, L. Wang and Y. Liao, Spirobifluorene-Based Conjugated Microporous Polymer-Grafted Carbon Nanotubes for Efficient Supercapacitive Energy Storage, *ACS Appl. Energy Mater.*, 2022, **5**, 3706–3714, DOI: **10.1021/acsaem.2c00151**.

64 Y. Dai, Y. Wang, H. Xu, X. Li, X. Yan and X. Xu, Structure, morphology and energy storage properties of imide conjugated microporous polymers with different cores and the corresponding composites with CNT, *Electrochim. Acta*, 2023, **441**, 141820, DOI: **10.1016/j.electacta.2023.141820**.

65 H. Zuo, J. Duan, B. Lyu, W. Lyu, Y. Li, X. Mei and Y. Liao, Carbon Nanotube Template-Assisted Synthesis of Conjugated Microporous Polytriphenylamine with High Porosity for Efficient Supercapacitive Energy Storage, *Macromol. Rapid Commun.*, 2023, 2300238, DOI: **10.1002/marc.202300238**.

66 L. Liu, D. Cui, S. Zhang, W. Xie, C. Yao and Y. Xu, Integrated carbon nanotube and triazine-based covalent organic framework composites for high capacitance performance, *Dalton Trans.*, 2023, **52**, 2762–2769, DOI: **10.1039/D2DT03910A**.

This journal is © The Royal Society of Chemistry 2023

J. Mater. Chem. A, 2023, **11**, 22868–22883 | **22883**